Research Square

Preprints are preliminary reports that have not undergone peer review.
They should not be considered conclusive, used to inform clinical practice,
or referenced by the media as validated information.

Transferability of single-layer hatch package experiments to multi-layer builds in beam-shaped laser-based powder bed fusion of metals for efficient parameter development

Robin Prudlik

robin.prudlik@tum.de

TUM School of Engineering and Design: Technische Universitat Munchen School of Engineering and Design https://orcid.org/0009-0005-7657-1330

Jonas Grünewald

TUM School of Engineering and Design: Technische Universitat Munchen School of Engineering and Design

Katrin Wudy

TUM School of Engineering and Design: Technische Universitat Munchen School of Engineering and Design

Research Article

Keywords: PBF-LB/M, Beam Shaping, Single Layer, Hatch Packages, Surface Topography, Melt Track Characteristics

Posted Date: November 9th, 2026

DOI: https://doi.org/10.21203/rs.3.rs-11296761/v1

License: This work is licensed under a Creative Commons Attribution 4.0 International License.
Read Full License

Transferability of single-layer hatch package experiments to multi-layer builds in beam-shaped laser-based powder bed fusion of metals for efficient parameter development

Author Name(s):

Robin Prudlik[1,2], Jonas Grünewald[1], Katrin Wudy[1]

Affiliation(s):

[1] *Technical University of Munich, Freisinger Landstrasse 52, 85748 Garching bei Muenchen, Germany*

[2] *Oerlikon AM Europe GmbH, Freisinger Landstrasse 52, 85748 Garching bei Muenchen, Germany*

Corresponding Author Email:

robin.prudlik@tum.de

Keywords

PBF-LB/M; Beam Shaping; Single Layer; Hatch Packages; Surface Topography; Melt Track Characteristics

Highlights

- Hatch packages transfer well to volumetric builds for shaped beams
- Flat and lack-of-fusion regimes show highest hatch package agreement
- Surface classifications transferable from hatch package to cube builds
- Hatch package melt track dimensions match multi-layer builds
- Beam-shaped hatch packages enable efficient parameter screening

Acknowledgement

The European Commission funded the research shown as part of the HORIZON program (Project 101058523 InShaPe). The authors are grateful for the financial funding. Additionally, the authors want to thank the project partner, EOS, for providing the system technology for the experiments.

Abstract

Beam shaping introduces additional flexibility in laser-based powder bed fusion of metals (PBF-LB/M) by enabling spatially tailored energy distributions. However, this increased degree of freedom significantly expands the process parameter space and complicates parameter development. While hatch package experiments have been shown to provide representative melt track characteristics of multi-layer builds in Gaussian-beam PBF-LB/M, their applicability to beam-shaped PBF-LB/M remains unclear. In this study, the transferability of hatch package experiments to multi-layer builds is investigated for beam-shaped processes. Surface topography, surface classification, and melt track characteristics obtained from single-layer hatch package experiments are compared with corresponding measurements from multi-track experiments using cube specimens. A strong correlation between hatch package and cube data is observed, with most hatch package surface classifications matching the corresponding classifications obtained from cube specimens. *Flat* and *Lack-of-Fusion* (*LoF*) regimes show particularly strong agreement, while *Bulging* and *Wavy* morphologies exhibit systematic deviations attributed to layer-wise interactions. Furthermore, melt track dimensions derived from hatch package experiments capture the trends observed in cube measurements, with coefficients of determination relative to the identity line of 0.895, 0.756, and 0.693 for depth, width, and area, respectively. Only melt track area shows consistently higher values for the hatch package compared to the cube measurements. Qualitative comparisons further confirm a strong agreement in spatial surface features and melt track geometry. Overall, hatch package experiments provide an efficient approach for assessing surface topography and melt track characteristics in beam-shaped PBF-LB/M, while highlighting limitations associated with the propagation of surface irregularities during multi-layer build-up.

1. Introduction

Beam shaping has emerged as a promising approach to expand the process capabilities of laser-based powder bed fusion of metals (PBF-LB/M). By enabling the spatial tailoring of the laser intensity distribution, beam shaping introduces an additional degree of freedom that allows targeted modification of melt pool behavior [1] or thermal gradients [2]. While this provides new opportunities for process optimization and control, it simultaneously increases the complexity of parameter development, as the parameter space is extended beyond conventional variables such as laser power and scan speed. Consequently, the experimental effort required for identifying suitable process conditions increases significantly.

Commonly, process parameter development in PBF-LB/M relies on simplified experimental approaches, such as single-track investigations [3]. However, it has been shown that single-track experiments are not representative of volumetric builds, as they fail to capture essential multi-track and multi-layer interactions governing the final component properties [4]. As a result, parameter sets derived from single-track analyses often do not translate reliably to part-scale production.

To address this limitation, hatch package experiments, i.e. single-layer scans consisting of multiple adjacent tracks, have been successfully applied in conventional PBF-LB/M with Gaussian beam profiles [5]. These experiments provide a more representative approximation of the steady-state melt track characteristics in volumetric builds.

However, it remains unclear whether this approach can be directly transferred to beam-shaped PBF-LB/M processes. In contrast to Gaussian intensity distributions, beam-shaped profiles, such as ring-shaped beams, exhibit fundamentally different spatial energy input characteristics, including multi-peak intensity distributions and enlarged interaction zones. These differences can significantly affect melt pool geometry, thermal gradients, and remelting behavior, potentially altering layer-wise interactions in comparison to conventional processes [6].

In particular, while hatch package experiments rely on the assumption that the dominant process conditions are established within a single layer and persist during subsequent deposition, this assumption may not hold for beam-shaped processes. The modified heat input distribution could lead to an altered time the steady-state process is reached, enhanced sensitivity to track overlap, altered melt pool dynamics, and increased influence of layer-wise accumulation effects.

To date, no systematic study has assessed whether hatch package experiments remain transferable to volumetric builds in beam-shaped PBF-LB/M. Therefore, the present study investigates the applicability of hatch package experiments for parameter development using beam-shaped laser intensity distributions. The objective is to evaluate whether top-surface topography, classification of top-surface topographies, and melt track characteristics obtained from hatch package experiments can reliably transfer to the behavior of multi-layer builds.

By establishing this relationship, this work aims to provide both a practical methodology for efficient parameter screening and a deeper understanding of the limitations of single-layer experiments in the context of advanced beam shaping strategies.

2. Materials and methods

This section describes the materials, experimental setup, and characterization methods used to assess the transferability of hatch package experiments to multi-layer builds in beam-shaped PBF-LB/M. Identical process parameter sets were applied to both hatch package specimens and cube builds, enabling a direct comparison of surface and melt track characteristics. The following subsections outline the material system, beam shaping implementation, experimental design, and the applied surface and metallographic characterization methods.

2.1. Material

Inconel 718 (IN718), a nickel-based superalloy commonly processed by PBF-LB/M due to its high-temperature strength and resistance to corrosion and creep, was used as feedstock material in this study. A gas-atomized IN718 powder supplied by Oerlikon Metco (US) Inc. was employed, corresponding to the commercial grade MetcoAdd™ 718C. The particle size distribution of the investigated batch, determined in accordance with ASTM B822, was characterized by $d_{10,3}$ = 20 µm, $d_{50,3}$ = 33 µm and $d_{90,3}$ = 51 µm. The nominal chemical composition of the powder is summarized in Table 1.

Table 1: Chemical composition of the used MetcoAdd™ 718C batch, characterized by Inductively Coupled Plasma Optical Emission Spectroscopy (ICP-OES).

Element	Ni	Cr	Fe	Nb+Ta	Mo	Ti	Al	Co	Si	Mn	Rest
Weight %	52.10	18.84	17.93	5.01	2.97	0.93	0.43	0.11	0.09	0.05	Bal.

2.2. System technology and beam shape characterization

All experiments were conducted on a modified commercial PBF-LB/M system (M290, EOS GmbH) equipped with a liquid-crystal-on-silicon (LCoS) spatial light modulator (SLM) for beam shaping. A 2 kW single-mode fiber laser (YLR-2000-SM, IPG Photonics) emitting at a wavelength of 1070 nm was used, with a minimum focal spot diameter of 90 µm in the Gaussian configuration. The LCoS-based optical setup enables phase-based wavefront modulation for generating tailored beam profiles as well as rotation of non-axisymmetric beam shapes relative to the scan direction.

Beam shape characterization was performed using a camera-based beam profiling system (FBP 2KF, CINOGY Technologies) with RayCi Pro software (v2.6.4). Ring-shaped beam profiles were characterized using a binary mask enclosing 86.47 % of the total beam energy. The mask was generated by ranking image pixels by intensity and selecting the minimum number required to reach the target energy fraction. This value corresponds to the energy enclosed within the standardized $1/e^2$ diameter of a Gaussian beam, providing a consistent basis for comparison. To reduce the influence of noise and boundary irregularities, the mask was smoothed using an adaptive median filter with a kernel size scaled to the equivalent diameter of the energy-enclosure region. The resulting mask was used for all subsequent geometric measurements. The centroid of the smoothed mask was determined and used as the origin of a polar coordinate system. A total of 720 radial rays, corresponding to an angular resolution of 0.5°, were projected over the full circumference. For each ray, the first and last intersections with the mask defined the inner and outer ring boundaries. Ring thickness was calculated as the radial distance between these boundaries, while the outer diameter was obtained as twice the distance from the centroid to the outer boundary. Mean values of ring thickness and outer diameter were calculated from all angular positions, enabling a robust characterization of annular beam profiles. The main algorithm steps are shown in Figure 1.

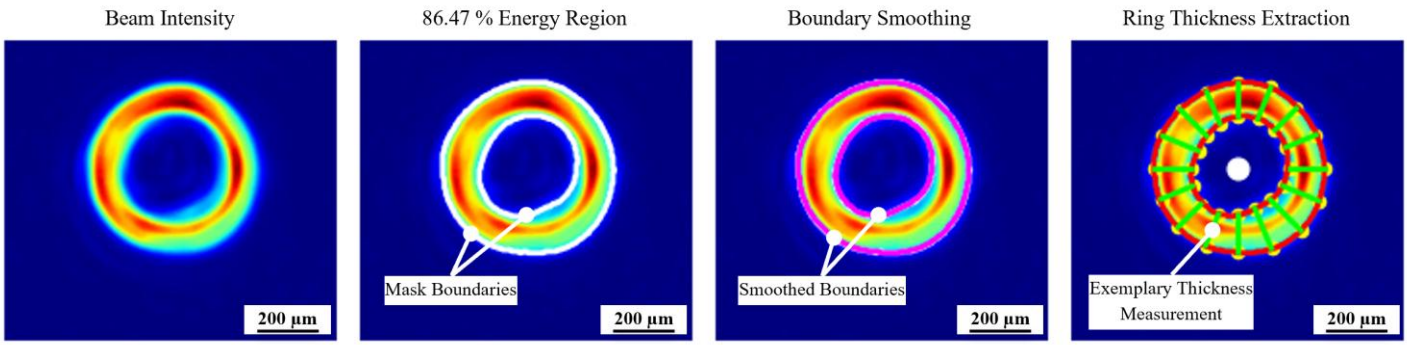


Figure 1: Main algorithm steps to determine the ring-shaped beam dimensions outer diameter and ring thickness.

2.3. *Experimental design*

Six ring-shaped beam configurations were investigated in this study, as ring profiles enable a more distributed energy input and are of particular industrial relevance due to their potential to improve process stability and productivity [7]. The selected beam profiles were defined based on the resolution capabilities of the beam shaping system, resulting in outer widths of 340 µm, 450 µm, and 560 µm. For the 340 µm configuration, ring widths (defined as the radial distance between the inner and outer intensity boundaries) of 100 µm and 125 µm were applied, while the 450 µm configuration included widths of 125 µm, 135 µm, and 155 µm. The 560 µm configuration was realized with a ring width of 115 µm. Throughout this work, the beam shapes are denoted using the nomenclature *Ring-"outer width"-"ring width"* (in µm). Figure 2 shows the intensity distribution in the working plane.

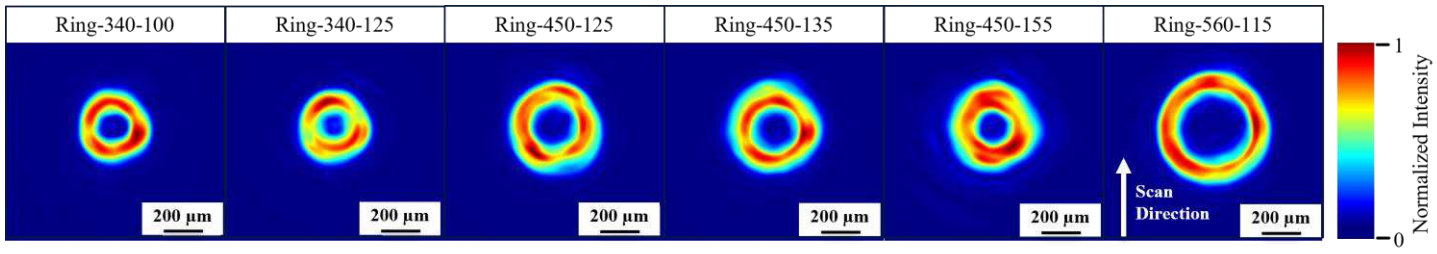


Figure 2: Intensity distribution in the working plane for the beam shapes used in this study. The ring configurations are denoted using the nomenclature *Ring-"outer width"-"ring width"*. The scanning direction is upwards.

For each beam configuration, a parameter matrix consisting of 18 distinct parameter sets was investigated and repeated three times, resulting in 54 specimens per configuration for both hatch packages and cube experiments, resulting in a total of 318 hatch packages and cubes. For the Ring-560-115 configuration, two parameter sets were omitted because they would have likely resulted in insufficient energy input. The process parameters laser power P_{Laser} and scan speed v_{Scan} were varied across three levels, while the hatch distance h was varied across two levels. Identical parameter matrices were applied for the 340 µm and 450 µm configurations, whereas the 560 µm configuration required an adapted parameter range due to its reduced energy input.

For each combination of laser power and scan speed, hatch distances were selected to cover process conditions associated with different surface topographies. All experiments were conducted using a constant layer thickness δ_{Layer} of 80 µm and a base-plate temperature T_0 of 80 °C. A summary of the investigated process parameters is provided in Table 2.

Table 2: Parameters used for the hatch package and cube experiments. Fixed parameters were a layer thickness δ_{Layer} of 80 µm, base plate heating T_0 of 80 °C and the material IN718.

Parameter	Ring-350-100, Ring-350-120, Ring-450-112, Ring-450-125, Ring-450-150								
Laser power P_{Laser} in W	700			1000			1300		
Scan speed v_{Scan} in mm/s	400	1200	2000	800	1600	2400	800	1600	2400
Hatch distance h in mm	0.15, 0.25	0.10, 0.15	0.10, 0.15	0.15, 0.25	0.10, 0.20	0.10, 0.20	0.15, 0.30	0.10, 0.25	0.10, 0.25
	Ring-550-100								
Laser power P_{Laser} in W	700			1000			1300		
Scan speed v_{Scan} in mm/s	800	1600	400	1200	2000	400	1200	2000	
Hatch distance h in mm	0.15, 0.20	0.10, 0.15	0.15, 0.40	0.15, 0.25	0.10, 0.20	0.15, 0.35	0.15, 0.30	0.10, 0.25	

2.4. Specimen design and layout

Hatch packages were produced on additively manufactured substrates with dimensions of 25 mm × 15 mm × 5 mm, onto which a successive powder layer with δ_{Layer} of 80 µm was applied. The substrates were fabricated using the standard process parameters provided by the machine manufacturer, employing a Gaussian beam with a diameter of 90 µm and parallel to gas flow direction. The hatch packages had dimensions of 3 mm in width and 12 mm in length and were oriented parallel to the gas flow direction. This resulted in minimum eight melt tracks, which exceeds the approximately three to four overlapping tracks reported by Templeton et al. [5] to reach steady-state melt pool conditions for IN718.

Cuboid specimens with lateral dimensions of 12 mm × 12 mm and a build height of 13 mm were manufactured for comparison. The specimens were oriented at 45° relative to the recoating direction. A layer-wise scan rotation of 90° combined with an initial offset of 45° was applied, ensuring alignment of the scan vectors with the specimen edges.

For the parameter set Ring-340-100, an additional stripe with a width of 4 mm was fabricated at the center of the cube top surface to enable direct comparison of melt track characteristics between hatch package and cuboid specimens. A bidirectional scanning strategy was applied consistently for both hatch packages and cube builds.

2.5. Top-surface measurements

The top-surfaces of all specimens were characterized using fringe projection (VR-3100, Keyence Corporation) operated at a magnification of 12×. This configuration provided a lateral resolution of 5 µm and a vertical resolution of 0.1 µm. All measurements were conducted in accordance with ISO 25178. For hatch package surfaces exhibiting adhered spatter on the top-surface, a short-wavelength cut-off of λ_s = 250 µm was applied. For the cube top-surfaces such spatters were not present, therefore omitting the filtering. The measurement region was positioned centrally on the top surface of each specimen and covered an area of 8 mm × 1.5 mm, ensuring a representative characterization of the surface topography, see Figure 3.

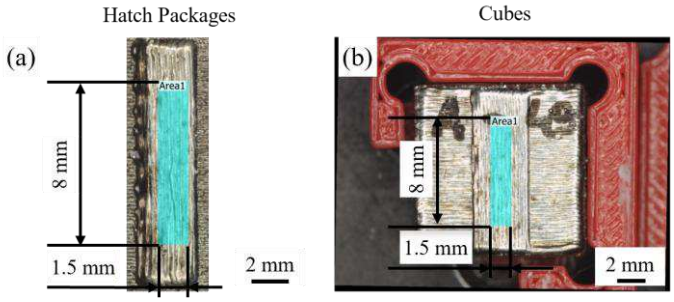


Figure 3: Surface measurement areas for (a) the hatch packages and (b) the cubes.

2.6. Top-surface characterization

Surface topography was classified based on a previously established methodology [8]. Four distinct surface topography classes were considered: *Flat*, *Bulging*, *Irregular*, and *Wavy*, where *Flat* and *Bulging* are defined as continuous and *Irregular* and *Wavy* as discontinuous surfaces. The classification was performed using a rule-based approach derived from areal surface parameters, namely the arithmetic mean height S_a, the autocorrelation length S_{al}, the developed interfacial area ratio S_{dr}, and the reduced peak height S_{pk} [8]. These parameters capture both amplitude- and spatial-related characteristics of the surface, enabling a consistent distinction between the different topography classes. The classification rules can be found in Table 3.

Table 3: Threshold rules for the different surface topography classes, result of [8].

Class	Threshold Rules
Continuous	$S_{pk} \geq 1206.75 \cdot S_{dr} - 48.68$
Discontinuous	$S_{pk} < 1206.75 \cdot S_{dr} - 48.68$
Flat	$S_{pk} \geq 1206.75 \cdot S_{dr} - 48.68$ AND $S_{al} < -91.12 \cdot S_a + 4269.50$
Bulging	$S_{pk} \geq 1206.75 \cdot S_{dr} - 48.68$ AND $S_{al} \geq -91.12 \cdot S_a + 4269.50$
Irregular	$S_{pk} < 1206.75 \cdot S_{dr} - 48.68$ AND $S_{dr} \geq 0.0076 \cdot S_a - 0.4437$
Wavy	$S_{pk} < 1206.75 \cdot S_{dr} - 48.68$ AND $S_{dr} < 0.0076 \cdot S_a - 0.4437$

2.7. Confusion matrix for transferability evaluation

To evaluate the transferability of single-layer hatch package measurements, the classification model previously developed for cube top-surface morphologies was directly applied to the measured surface parameters obtained from the hatch package specimens. Since the objective is to assess whether hatch package specimens exhibit the same surface topography classes as the corresponding cube builds, the resulting class assignments were compared using a confusion matrix. The confusion matrix quantifies the agreement between hatch package and cube classifications by showing how frequently specimens are assigned to the same class and where misclassifications occur. Entries along the diagonal represent cases in which hatch package and cube specimens are assigned to the same surface morphology class, indicating successful transferability, whereas off-diagonal entries correspond to transitions between different classes and thus highlight deviations between single-layer and multi-layer behavior. Both absolute sample counts and relative frequencies are reported to provide a comprehensive assessment of classification agreement and transferability.

2.8. Metallurgical preparations

For melt track analysis, specimens were sectioned along the build direction and perpendicular to the scan direction of the top layer using a precision cutting machine (Secotom-50, Struers ApS). The samples were subsequently mounted in conductive Bakelite using a hot mounting press (CitoPress-30, Struers ApS). Metallographic preparation was carried out by sequential grinding with SiC papers (#320, #500, and #1000), followed by diamond polishing using suspensions with particle sizes of 9 µm and 3 µm. A final polishing step was performed using a 0.25 µm silica-based suspension on an automatic grinding and polishing system (Tegramin-30, Struers ApS). The microstructure was revealed by electrochemical etching using a 10 % phosphoric acid solution at an applied voltage of 3.1 V.

2.9. *Melt track characterization*

The melt track geometry was evaluated based on cross-sectional analyses, as shown in Figure 4. All the measurements were taken on the last track of the hatch package. The melt track width w_{MT} was defined as the lateral distance between the two triple points at the surface, where the melt track boundary intersects the surrounding material. The melt track depth δ_{MT} was measured at the midpoint of the determined width. From this location, the depth was evaluated perpendicular until the lowest point of the melt track boundary was reached. The melt track area A_{MT} was determined by integrating the enclosed region defined by the melt track contour. For this purpose, the boundary of the melt track was manually outlined, and the corresponding cross-sectional area was calculated.

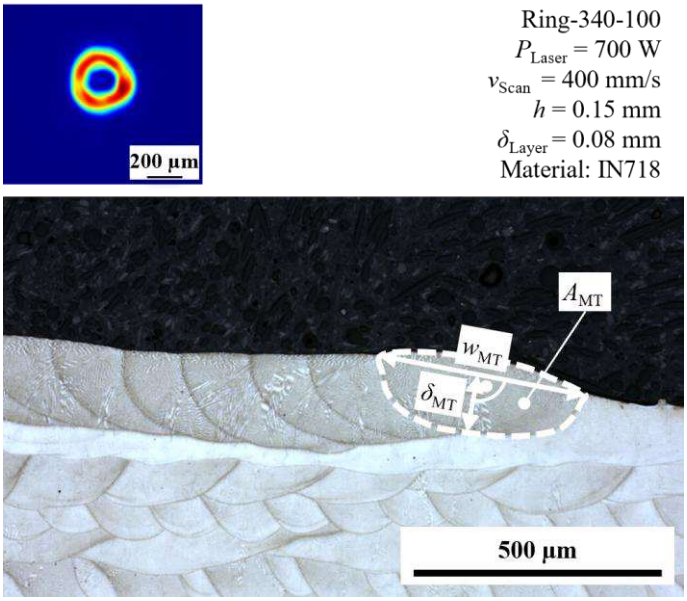


Figure 4: Melt track measurements sketch for the melt track depth δ_{MT}, width w_{MT}, and area A_{MT} on IN718 using the Ring-340-100, a laser power P_{Laser} of 700 W, scan speed v_{Scan} of 400 mm/s hatch distance h of 0.15 mm and layer thickness δ_{Layer} of 0.08 mm.

3. Results and discussion

The following section presents the comparison between hatch package experiments and corresponding cube builds with respect to surface topography and melt track geometry. First, the transferability of areal surface parameters and resulting surface topographies is evaluated, followed by an assessment of the transferability of hatch package-based surface classification. Subsequently, the agreement in melt track geometry between single-layer and multi-layer conditions is analyzed. The results are discussed in the context of the underlying process mechanisms governing layer-wise interactions and their influence on the final surface and melt track geometry.

3.1. Comparison of surface parameters and top-surface topography

Figure 5 shows the comparison of the areal surface roughness S_a between hatch package and cube measurements for different surface topographies, revealing a strong dependence of the agreement on the respective surface class. The surface classes correspond to the classes observed for the cube specimens for the respective process parameters.

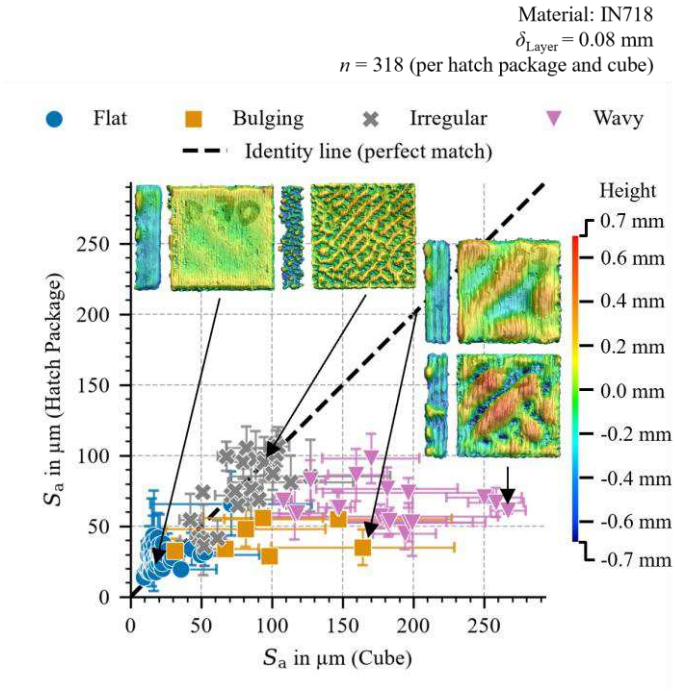


Figure 5: Comparison of surface parameter S_a between hatch packages and cube measurements for the investigated parameter combinations using ring-shaped beams. The surface classes correspond to the classes observed for the cube specimens for the respective process parameters.

For cube samples classified as *Flat*, both the cube and hatch package measurements show a generally close correspondence, with data points clustering around the identity line. However, the observed deviations are not negligible, with a mean deviation of 7.7 µm ± 9.7 µm (25.9 % ± 30.6 %), corresponding to a noticeable fraction of the absolute roughness values. This indicates that while the surface characteristics captured in the single-layer hatch package experiments are broadly representative of the final surface state, quantitative differences remain for this regime. S_a is systematically larger for *Bulging* surfaces when comparing cube measurements to hatch package data. *Irregular* surfaces exhibit a larger scatter compared to the *Flat* regime; however, the data remain predominantly distributed around the identity line, suggesting a moderate but consistent agreement between hatch package and cube measurements, with a mean deviation of -0.6 µm ± 18.6 µm (-3.8 % ± 25.5 %). In contrast, *Wavy* surfaces show the largest deviations from the identity line, indicating a substantial increase in roughness in the cube specimens relative to the single-layer hatch package reference. Overall, the results demonstrate that S_a values obtained from hatch packages and cubes are most similar for *Flat* and *Irregular* surface

topographies. In these regimes, it seems that the dominant surface features are largely established within the first layer and are not significantly altered during subsequent layer deposition.

In contrast, the systematically smaller S_a values for *Bulging* and *Wavy* surfaces in the hatch packages indicate that additional mechanisms become relevant during the build-up of multiple layers. Specifically, defect propagation in the build direction leads to a progressive modification of the surface topography, where small geometrical irregularities formed in early layers can evolve into larger defect structures extending over multiple layers, as demonstrated by Bauereiß et al. [9]. Such defects may persist due to melt redistribution and incomplete remelting. However, even in the absence of these defects, significant surface irregularities can arise from intrinsic process dynamics, as stochastic powder deposition and melt pool motion induce pronounced height variations. As a result, geometric deviations are not only propagated but also amplified over successive layers, leading to increasingly irregular local layer thicknesses and a growing discrepancy between hatch package and cube-derived roughness.

The comparison of the spatial roughness parameter S_{al}, which describes the wavelength content of the surface, between hatch package and cube measurements reveals distinct trends depending on the surface topography, see Figure 6.

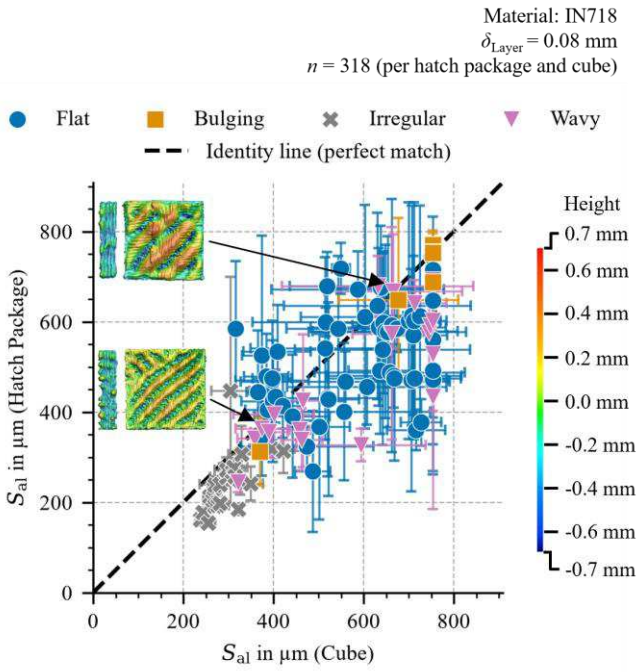


Figure 6: Comparison of surface parameter S_{al} between hatch packages and cube measurements for the investigated parameter combinations using ring-shaped beams. The surface classes correspond to the classes observed for the cube specimens for the respective process parameters.

For samples classified as *Flat*, a pronounced scatter around the identity line is observed. This behavior can be attributed to the inherent sensitivity of S_{al} to small topographical variations. In the absence of pronounced surface features, even minor perturbations in the surface structure lead to significant fluctuations in the characteristic lateral length scale, resulting in a comparatively broad spread of the data. In contrast, *Bulging* surfaces exhibit a substantially stronger agreement between hatch package and cube measurements. While the values of S_{al} for the hatch packages are systematically slightly lower compared to the cubes, the overall transferability remains strong, indicating that the dominant surface wavelength is largely maintained in many cases during the transition from single-layer to multi-layer builds, with a mean deviation of -19 µm ± 31.7 µm (-4.3 % ± 7.3 %). A comparably strong agreement is found for *Irregular* surfaces. In this regime, the scatter is notably reduced, and both hatch package and cube measurements are associated with comparatively small error bars. The data clusters slightly below the identity line, reflecting a stable and well-defined characteristic length scale. The slightly lower values observed for the cube measurements suggests only minor modifications of the surface topography during layer

build-up, with a mean deviation of -67.3 µm ± 32.9 µm (-31.7 % ± 19.5 %). For *Wavy* surfaces, most data points lie below the identity line, indicating a general increase of S_{al} in the cube measurements compared to the hatch package reference. Nevertheless, the overall agreement remains strong, as the points still follow the expected trend. This indicates that while the absolute magnitude of the characteristic wavelength is increased, the underlying surface pattern is consistently transferred into the multi-layer geometry.

In summary, the results demonstrate that the lateral surface characteristic S_{al} can be reasonably transferred across most surface classes using hatch package-derived data. However, its sensitivity to small-scale topographical variations leads to increased scatter for *Flat* surfaces, whereas for more structured topographies such as *Bulging*, *Irregular*, and *Wavy*, the parameter exhibits a more robust and transferrable behavior.

To further demonstrate the relationship between hatch package and cube measurements, exemplary top surface images of cube specimens are overlaid with the corresponding spatial regions extracted from single-layer hatch package measurements in pseudo colors, see Figure 7. Across all surface topographies shown, a very strong agreement in the spatial distribution of surface elevations can be observed. Characteristic features such as ridges, valleys, and periodic structures identified in the hatch package measurements are consistently reproduced in the cube top-surfaces. These observations suggest that key features of the surface topography are already present after the initial layer, although their evolution over subsequent layers cannot be directly resolved in this study. The results demonstrate that hatch package measurements provide a representative description of the spatial distribution of elevations, and thus surface topography, that ultimately manifests in the additively manufactured component.

The observed transferability between hatch package experiments and cube builds can be interpreted in the context of the spatial energy distribution inherent to the employed ring-shaped beam profiles. Compared to Gaussian beams, ring-shaped intensity distributions result in a broader lateral energy input with reduced peak intensity, which tends to promote more stable and distributed melt track geometries [6]. In regimes such as *Flat* and *Irregular*, the melt track geometry is primarily governed by the effective energy input and track overlap conditions, which are largely established during the formation of the first layer. As a result, the characteristic surface features and melt track dimensions are defined at this stage and remain relatively stable during subsequent layer deposition.

In contrast, regimes such as *Bulging* and *Wavy* are associated with increased melt pool instability due to less lateral confinement [10], local variations in material accumulation, and deviations in effective layer thickness [9]. These effects are amplified over multiple layers through feedback mechanisms, including uneven powder spreading and variation in remelting conditions [9]. As these layer-wise interactions are not captured in single-layer experiments, deviations between hatch package and cube measurements are more pronounced for these topographies. This highlights the inherent limitation of hatch package experiments in capturing cumulative process instabilities.

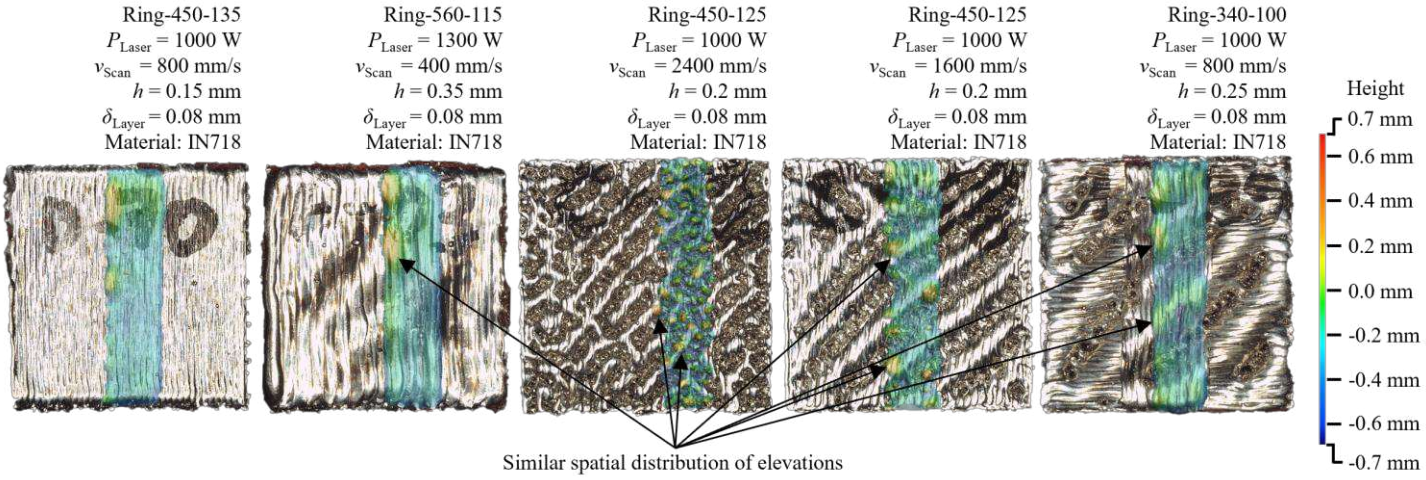


Figure 7: Visual comparison of a hatch package surface topography, shown in pseudo-colors, on a respective cube top-surface for the same process parameters.

The confusion matrix shown in Figure 8 compares the surface topography classifications obtained from hatch package and cube specimens. Diagonal entries represent matching classifications, whereas off-diagonal entries indicate transitions between different surface topography classes. The matrix reveals a strong agreement between observed surface classes of hatch packages and cubes, as indicated by the dominant counts along the diagonal. This demonstrates that, in most cases, the top-surface topography of volumetric cube specimens can be reliably transferred from the corresponding hatch package measurements.

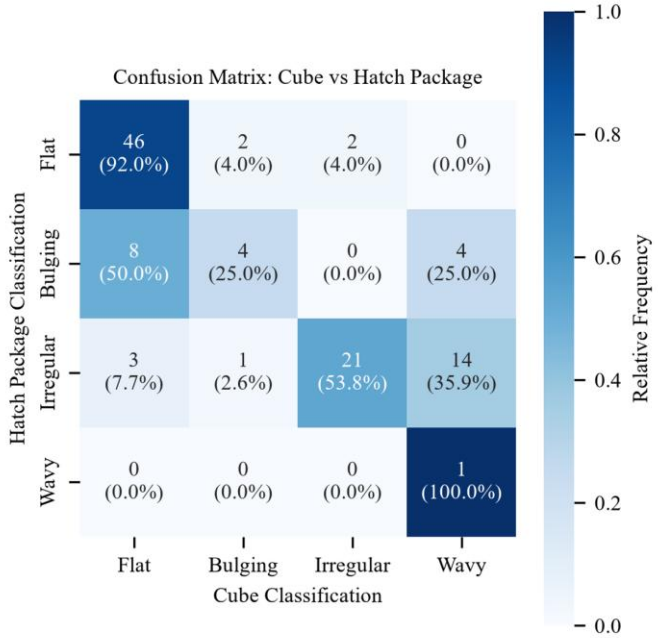


Figure 8: Confusion matrix showing the predictive accuracy from hatch package to cube top-surface classes.

In particular, *Flat* hatch package surfaces lead to *Flat* cube top-surface morphologies in 92 % of the cases, with the remaining samples predominantly classified as *Bulging*. Only two cases (4.0 %) resulted in a discontinuous top-surface topography, highlighting the robustness of the classification in this regime. In contrast, *Bulging* hatch package surfaces exhibit a broader distribution across the resulting cube classes, with significant fractions assigned to *Flat*, *Bulging*, and *Wavy* topographies. Notably, the largest share of *Bulging* hatch package samples transitions into *Flat* cube top-surfaces. This behavior suggests that *Bulging* conditions are sensitive to layer-wise

interactions and should therefore be considered in more detail when extrapolating hatch package results to volumetric builds. Under certain circumstances the surface irregularities, consisting of peaks and valleys, may cancel each other out, therefore "healing" the surface irregularities in multi-layer builds.

For *Irregular* conditions, a generally strong agreement between hatch package and cube classifications is observed, although some misclassifications occur. The confusion with *Wavy* topographies can be attributed to the limited representation of roughness amplitude in single-layer measurements. Since the distinction between *Irregular* and *Wavy* regimes strongly depends on S_a, the reduced vertical extent captured in hatch package measurements can lead to ambiguity in the classification. Nevertheless, the majority of *Irregular* hatch package samples correctly result in *Irregular* cube top-surfaces, confirming the validity of the approach for this regime.

The *Wavy* class is only sparsely represented in the hatch package dataset; however, the single *Wavy* hatch package sample is correctly mapped to a *Wavy* cube top-surface, indicating consistency in this regime. It is also worth noting that prior investigations [8] have shown that *Flat* surface topographies are typically associated with high relative densities. While density was not assessed in this study, this relationship suggests that hatch package-based surface predictions may serve as an indicator for suitable process conditions during parameter development.

Overall, the confusion matrix highlights that the classification derived from hatch package measurements is largely transferable to cube surface topography across most regimes. However, it should be noted that amplitude-based surface parameters depend on the number of deposited layers, as roughness is progressively modified by layer-wise accumulation effects, including defect propagation, stochastic powder deposition, and melt pool dynamics [9]. Consequently, discrepancies between hatch package and cube measurements increase for regimes characterized by pronounced surface irregularities, such as *Bulging* and the transition between *Irregular* and *Wavy*.

3.2. Comparison of melt track dimensions

Following the surface-based analysis, the comparison is extended to the melt track geometry. The melt track dimensions obtained from hatch package experiments are compared with those extracted from the corresponding cube-hatch package specimens. The analysis is restricted to the Ring-340-100 configuration, for which a consistent and representative dataset is available across both experimental configurations. Although this limits the generalization of melt track transferability across all beam profiles, prior studies have shown that melt track geometry is primarily governed by the spatial energy distribution and characteristic length scale of the beam [11]. Consequently, beam profiles with comparable dimensions and energy input characteristics tend to exhibit similar melt track behaviour in terms of width, depth, and overall geometry [6]. This allows qualitative trends observed for the selected configuration to be transferred to other beam shapes within the same size regime, while maintaining a controlled comparison between single-layer and multi-layer conditions. The comparison of melt track geometry between hatch package and cube specimens reveals a generally strong agreement across the investigated metrics, see Figure 9.

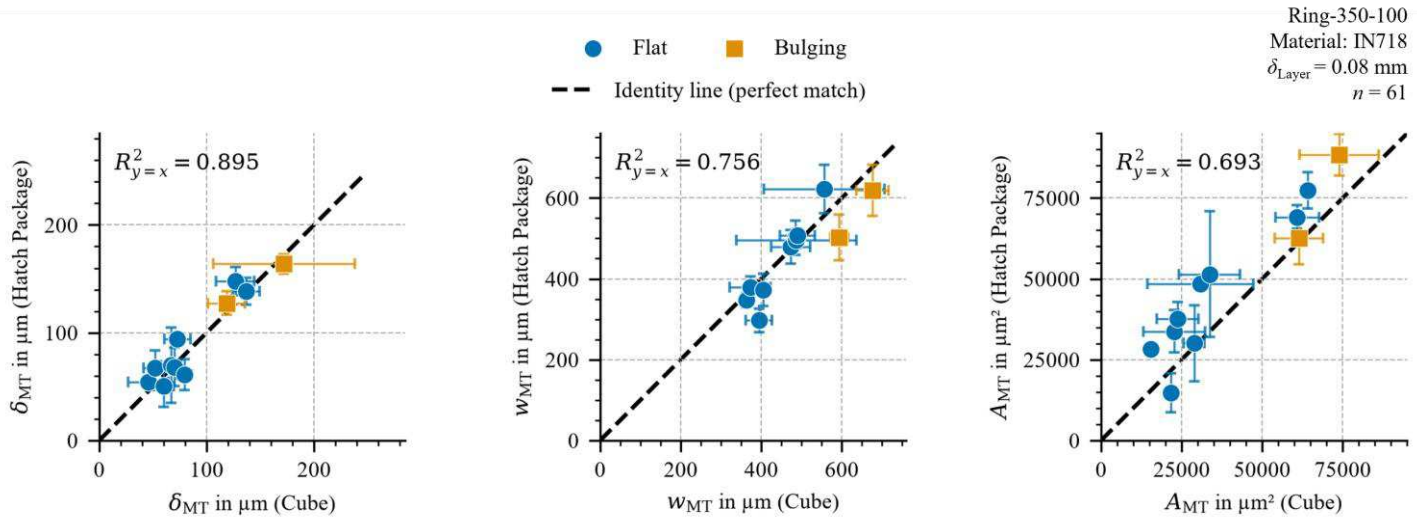


Figure 9: Comparison of melt track dimensions melt track depth δ_{MT}, width w_{MT}, and area A_{MT} between hatch package and cube experiment on IN718 using the Ring-340-100.

The correspondence between both approaches is reflected in the coefficient of determination with respect to the identity line, yielding $R^2_{y=x} = 0.895$ for the melt track depth, 0.756 for the melt track width, and 0.693 for the melt track area. These values indicate that the melt track depth can be correlated with high accuracy, while width and area still exhibit strong, albeit slightly reduced, agreement.

A systematic deviation is only observed for the melt track area, which tends to be lower in the cube-hatch package measurements compared to the hatch package reference. This suggests that while the fundamental melt track dimensions are largely preserved during the transition from single-layer to multi-layer builds, the combined effect of width and depth variations leads to a moderate increase in the measured melt track area.

These findings demonstrate that not only the top-surface topography but also the underlying melt track geometry can be reliably transferred using hatch package experiments. This highlights the capability of single-layer measurements to capture key process-structure relationships relevant for volumetric builds.

This conclusion is further supported by the exemplary melt track cross-sections shown in Figure 10, where a close resemblance in melt track geometry between hatch package and cube specimens can be observed across different process parameter combinations. Characteristic features such as melt track shape, penetration depth, and lateral extent are consistently reproduced, indicating that the primary melt track geometry is governed during initial layer formation and remains largely stable throughout subsequent build-up.

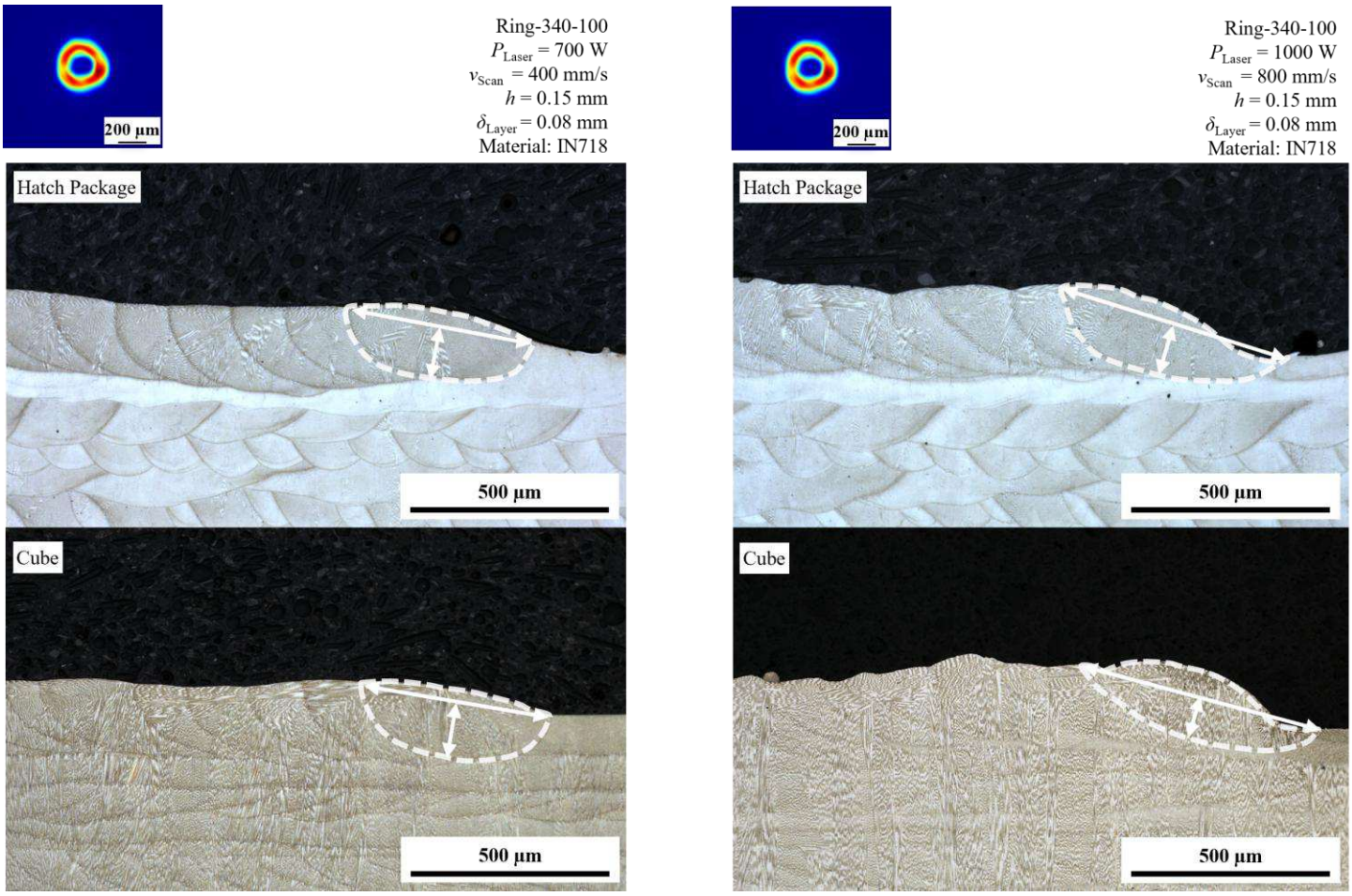


Figure 10: Visual comparison of hatch package and cube melt track geometry. The white arrows indicate the measurements for the melt track depth δ_{MT} and width w_{MT}, while the dashed contour outlines the melt track and is used for calculating the melt track area A_{MT}.

The findings of this study should be considered with several limitations. The experiments were conducted using a single material (IN718) and a fixed layer thickness of 80 µm, which may limit the direct transferability of the results to other materials or process conditions. Melt track characterization was restricted to a single beam configuration and therefore does not capture the full range of possible beam-shaping effects. Finally, the *Wavy* regime is underrepresented in the dataset, which restricts the statistical significance of observations for this topography class. Despite these limitations, the results indicate that single-layer hatch package experiments can substantially reduce the effort required for parameter development, as the high degree of transferability allows relevant process windows to be identified without performing extensive multi-layer builds. This makes hatch package-based approaches particularly effective for rapid parameter screening, while additional validation remains necessary for regimes influenced by layer-wise accumulation effects.

4. Conclusion

This study systematically assessed the transferability of surface topography and melt track geometry from single-layer hatch package experiments to multi-layer cube builds using ring-shaped beam profiles. It demonstrated the validity of hatch packages as a high-throughput approach for process development with IN718 and a layer thickness of 0.08 mm. To this end, identical process parameters were applied to both the hatch packages and cubes, and the resulting surface topographies and melt track geometries were compared using areal surface metrics, a rule-based classification approach, and cross-sectional analyses. Across the parameter sets investigated, which covered a wide range of changes in laser power, scan speed, hatch distance and beam profiles, a strong agreement was observed between hatch package-derived and cube-derived metrics for both surface descriptors and melt track geometry. In particular, the cube top-surface topography could be transferred with high accuracy for specific surface regimes using hatch package data, as confirmed by the high classification accuracy and the dominance of diagonal elements in the confusion matrix. Furthermore, melt track dimensions extracted from hatch package experiments showed close correspondence with those measured in cube specimens, particularly for melt track depth. The results can be summarized as follows:

- Strong agreement between hatch package- and cube-based top-surface classifications confirms the transferability of the classification framework, as demonstrated by the confusion matrix.
- Surface roughness and spatial characteristics for *Flat* and *Irregular* surfaces could be transferred well, indicating that their defining features are largely established during the initial layer formation.
- *Bulging* and *Wavy* specimens show lower surface parameter values in hatch package measurements, as amplitude-based classification metrics accumulate over multiple layers due to defect propagation and evolving surface topography.
- Melt track depth, width, and area exhibit substantial agreement between both the hatch package and cube measurements, with identity-line coefficients of determination of 0.895, 0.756, and 0.693, respectively. While melt track depth shows the highest transferability, the lower coefficient of determination for melt track area indicates a greater sensitivity to geometric variations between single-layer and multi-layer builds.
- The qualitative comparison of melt track cross-sections confirms that characteristic geometric features are preserved from single-layer to multi-layer builds.

The results, using a wide range of process parameters and ring-shaped beam profiles, indicate that single-layer hatch package experiments provide an efficient framework for predicting both surface topography and melt track characteristics in volumetric builds using beam shaping, with limitations depending on top-surface topography. This significantly reduces experimental effort compared to full 3D builds and enables rapid exploration of process parameter spaces. In particular, the ability to reliably predict *Flat* and *Irregular* regimes offers valuable insights for process optimization toward high-density components.

At the same time, the observed deviations for *Bulging* and *Wavy* morphologies highlight the importance of considering layer-wise accumulation effects when translating hatch package results to volumetric manufacturing. These findings therefore not only demonstrate the applicability of hatch package-based approaches but also delineate their limitations, providing a clear basis for more efficient parameter development in PBF-LB/M.

Declaration of generative AI and AI-assisted technologies in the writing process

During the preparation of this work the author(s) used Microsoft Copilot in order to improve language and readability. After using this tool/service, the author(s) reviewed and edited the content as needed and take(s) full responsibility for the content of the published article.

5. References

[1] A. R. Bakhtari, H. K. Sezer, O. E. Canyurt, O. Eren, M. Shah, and S. Marimuthu, "A Review on Laser Beam Shaping Application in Laser‐Powder Bed Fusion," *Adv Eng Mater*, vol. 26, no. 14, 2024, Art. no. 2302013, doi: 10.1002/adem.202302013.

[2] R. Shi, S. A. Khairallah, T. T. Roehling, T. W. Heo, J. T. McKeown, and M. J. Matthews, "Microstructural control in metal laser powder bed fusion additive manufacturing using laser beam shaping strategy," *Acta Materialia*, vol. 184, pp. 284–305, 2020, doi: 10.1016/j.actamat.2019.11.053.

[3] A. Bauch, P. Kohlwes, and I. Kelbassa, "Laser powder bed fusion of pure copper using ring-shaped beam profiles," *Journal of Laser Applications*, vol. 36, no. 4, 2024, Art. no. 042021, doi: 10.2351/7.0001562.

[4] T. M. Wischeropp, H. Tarhini, and C. Emmelmann, "Influence of laser beam profile on the selective laser melting process of AlSi10Mg," *Journal of Laser Applications*, vol. 32, no. 2, p. 22059, 2020, doi: 10.2351/7.0000100.

[5] F. Templeton William, H. Shawn, S. Seth, T. Albert, and N. Sneha Prabha, "Finding the limits of single-track deposition experiments: An experimental study of melt pool characterization in laser powder bed fusion," *Materials & Design*, vol. 231, p. 112069, 2023, doi: 10.1016/j.matdes.2023.112069.

[6] F. Nahr, D. Bartels, R. Rothfelder, and M. Schmidt, "Influence of Novel Beam Shapes on Laser-Based Processing of High-Strength Aluminium Alloys on the Basis of EN AW-5083 Single Weld Tracks," *JMMP*, vol. 7, no. 3, p. 93, 2023, doi: 10.3390/jmmp7030093.

[7] A. Ullah *et al.,* "Advancing laser powder bed fusion of metals via tailored laser beam shaping: A critical review," *Materials & Design*, vol. 268, p. 116548, 2026, doi: 10.1016/j.matdes.2026.116548.

[8] R. Prudlik, J. Grünewald, S. Sankaré, and K. Wudy, "Machine learning based surface topography classification in laser-based powder bed fusion of metals using beam shaping," *Additive Manufacturing Letters*, vol. 18, p. 100389, 2026, doi: 10.1016/j.addlet.2026.100389.

[9] A. Bauereiß, T. Scharowsky, and C. Körner, "Defect generation and propagation mechanism during additive manufacturing by selective beam melting," *Journal of Materials Processing Technology*, vol. 214, no. 11, pp. 2522–2528, 2014, doi: 10.1016/j.jmatprotec.2014.05.002.

[10] Z. Taylor *et al.,* "Analytical model for balling defects in laser melting using rivulet theory and solidification," *Journal of Applied Physics*, vol. 139, no. 2, 2026, Art. no. 024902, doi: 10.1063/5.0263633.

[11] L. Chechik, K. Schwarzkopf, R. Rothfelder, J. Grünewald, and M. Schmidt, "Material dependent influence of ring/spot beam profiles in laser powder bed fusion," *Additive Manufacturing Letters*, vol. 9, p. 100211, 2024, doi: 10.1016/j.addlet.2024.100211.

Statements and Declarations

Funding

The European Commission funded the research shown as part of the HORIZON program (Project 101058523 InShaPe). The authors are grateful for the financial funding.

Competing Interests

The authors declare that they have no known competing financial interests or personal relationships that could have appeared to influence the work reported in this paper.

CRediT Author Contributions

Robin Prudlik: Conceptualization, Methodology, Software, Formal analysis, Investigation, Data Curation, Writing - Original Draft, Writing - Review & Editing, Visualization

Jonas Grünewald: Writing - Review & Editing

Katrin Wudy: Writing - Review & Editing, Supervision, Project administration, Funding acquisition